Sensors & Actuators: B. Chemical 290 (2019) 426–433

Contents lists available at ScienceDirect

Sensors and Actuators B: Chemical

journal homepage: www.elsevier.com/locate/snb

Ppb-level nitric oxide photoacoustic sensor based on a mid-IR quantum cascade laser operating at 52 °C

Hongpeng Wu[a,b,1], Xukun Yin[a,b,e,1], Lei Dong[a,b,*], Zhiwei Jia[c,d], Jinchuan Zhang[d], Fengqi Liu[d], Weiguang Ma[a,b], Lei Zhang[a,b], Wangbao Yin[a,b], Liantuan Xiao[a,b], Suotang Jia[a,b], Frank K. Tittel[e]

[a] State Key Laboratory of Quantum Optics and Quantum Optics Devices, Institute of Laser Spectroscopy, Shanxi University, Taiyuan, 030006, China
[b] Collaborative Innovation Center of Extreme Optics, Shanxi University, Taiyuan, 030006, China
[c] College of Physics and Optoelectronics, Taiyuan University of Technology, Taiyuan, 030024, China
[d] Key Laboratory of Semiconductor Materials Science, Institute of Semiconductors, Chinese Academy of Sciences, Beijing, 100083, China
[e] Department of Electrical and Computer Engineering, Rice University, 6100 Main Street, Houston, TX, 77005, USA

ARTICLE INFO

Keywords:
Nitric oxide detection
Photoacoustic spectroscopy
High temperature continuous-wave DFB-QCL
Outdoor environmental monitoring

ABSTRACT

A ppb-level nitric oxide (NO) photoacoustic sensor was reported for outdoor environmental monitoring. The sensor employed a continuous wave (CW), distributed feedback (DFB), mid-infrared (mid-IR) quantum cascade laser (QCL) operating at a high temperature of 52 °C, which allow avoiding any water-cooling systems and thereby reduces its size, weight and cost of the photoacoustic NO sensor. The QCL emits at 5.26 μm, which corresponds to a strong NO absorption doublet *R*(6.5). A differential photoacoustic cell was designed to operate together with the QCL, resulting in a detection sensitivity of ~7 ppb at atmospheric pressure with a 1-s averaging time. An Allan–Werle deviation analysis indicated that a ppt-level detection sensitivity can be reached with an integration time of > 100 s. The performance of this sensor system was evaluated in terms of humidity, linearity and stability. Continuous measurements covering a haze period were performed to demonstrate the stability and robustness of the reported NO sensor system.

1. Introduction

Nitric oxide (NO), together with sulfur oxides, carbon monoxide and volatile organic compounds are primary pollutants in the atmosphere [1,2]. Industrial combustion processes as well as vehicle exhaust emissions constitute the main source of NO in the atmosphere. NO detection is of interest in the field of environmental monitoring because of its function in atmospheric chemistry, which results in acid rain, chemical smog and ozone reduction. In addition, there is an increasing need for the sensitive and selective detection of NO in diverse application fields that include industrial process control, combustion studies and noninvasive medical diagnostics [3,4].

Conventional method for determining NO concentration is chemiluminescence [4]. However, laser-based methods are being implemented more frequently since they offer fast and real-time monitoring capabilities with excellent sensitivity [5–9]. For laser-based trace gas sensor, efficient detection can be pursued essentially by selecting the most suitable spectral absorption range. In the case of NO detection, the optimum wavelength range between 5.07 μm and 5.73 μm provides nearly 500 times stronger absorption lines in comparison to near-infrared (1.79 μm–1.82 μm) wavelengths, offering low interference from other species (mostly water vapor and carbon monoxide) [10]. Quantum-cascade lasers (QCLs), whose performance have been improved significantly since their first report in the 1990s, represent the most promising light source in this wavelength range [11,12]. A single-mode, continuous-wave (CW) QCL has the best potential for gas sensing applications due to its compact size, narrow linewidth, wavelength tunability as well as its straightforward operation [13–16].

Several NO gas sensors using a mid-infrared (mid-IR) CW QCL as light source have been reported in the literature. The detection sensitivity of these NO sensors can usually achieve ppb concentration levels and even lower, which is sufficient for environmental monitoring. However, the QCL operating conditions differ greatly from sensor to sensor. This is also pertinent for the photodetectors in these sensors. Kosterev et al. [7] developed a ppb-level NO gas sensor by means of cavity ring-down spectroscopy (CRDS). Both the CW, distributed feedback (DFB) QCL and the photovoltaic HgCdTe detector in this sensor

* Corresponding author.
E-mail address: donglei@sxu.edu.cn (L. Dong).
[1] These authors contributed equally to this work.

https://doi.org/10.1016/j.snb.2019.04.007
Received 25 January 2019; Received in revised form 1 April 2019; Accepted 2 April 2019
Available online 03 April 2019
0925-4005/

were operated with liquid-nitrogen cooling. Bakhirkin et al. [8] reported a NO sensor based on off-axis integrated cavity output spectroscopy (OA-ICOS). The sensor utilized a CW, DFB-QCL operating at liquid-nitrogen temperature and a sensitive HgCdZnTe photodetector. Lewicki et al. [17] exploited Faraday rotation spectroscopy (FRS) based sensors for NO detection using a CW external cavity (EC) QCL operating at −20 °C. The performance of the FRS sensors equipped with a thermoelectrically cooled (TEC) HgCdTe photodetector and a liquid nitrogen-cooled InSb photodetector were evaluated, respectively. Recently, Yu et al. [5] demonstrated a ppb-level NO sensor using a CW, DFB-QCL and 76-m multipass gas cell. The temperature of the TEC QCL was controlled at 19.5 °C and simultaneously the HgCdTe detector temperature was stabilized at ~-60 °C via 3-stage TE cooling.

In mid-IR laser-based NO sensor systems reported to date, the employed CW QCLs are usually operated in a temperature range from liquid-nitrogen temperature to room temperature, which was mainly limited by their tunable wavelength range and output power. Therefore, a supplementary equipment for QCL temperature control, such as a water chiller, must be employed, when the sensor system is exposed to an outdoor environment. This adds inevitable bulkiness to the sensor system. Moreover, a high temperature conditions in summer must be taken into account in many area of China. For example, in the Shenzhen area, China, temperatures reach > 30 °C during 100 days per year and the surface temperature in summer can be > 60 °C. It is a challenge to cool a QCL in such a high ambient temperature environment down to room temperature or lower in the presence of a self-heating effect, in which QCLs release a large amount of heat to cause its own temperature increase due to their low wall-plug efficiency (WPE) [18]. Furthermore at a temperature of 30 °C and an 80% relative humidity, the dew point is 26 °C. Condensation of water vapor occurs at the QCL housing and window when the QCL temperature is controlled below room temperature. Hence, a good solution for a QCL working in a harsh outdoor environment is to operate the QCL at a high temperature (> 50 °C), as a heating process is more efficient and easier than a cooling process. Moreover, the heat release from QCL itself can assist the temperature control system to reduce the power requirement for heating, thereby realizing a compact robust mid-IR sensing system with a low electrical power consumption.

The optical detector in the mid-IR spectral range also plays an important role in a laser absorption spectroscopy (LAS) based NO sensor system. To improve the detection sensitivity, cryogenic cooling by means of a liquid nitrogen or water-cooled method is required for a costly mid-IR detector, as mentioned above. Photoacoustic spectroscopy (PAS) is an alternative technique, which can remove the requirement of an optical detector in a laser-based gas sensor system [19–22]. A PAS-based sensor converts the acoustic wave created by gas absorption of a laser beam into an electrical signal via an acoustic transducer such as a microphone [23,24] or a quartz tuning fork [25–27]. The target gas concentration is proportional to the amplitude of the PAS detection signal.

In this manuscript, we report the development of a sub-ppb level NO sensor system for outdoor environmental monitoring. The sensor employed a CW, DFB-QCL emitting at 5.26 μm and operating at 52 °C. The working capacity of the QCL at high temperature allows a totally thermoelectrically cooled mid-IR laser source, which reduces the sensor size, weight and cost. A custom-made differential photoacoustic cell with a λ/4 filter and buffer volume was designed in order to suppress the background noise level and thereby improve the detection sensitivity. The combination of the low noise PAS system and a high temperature QCL offers a highly sensitive, cost-efficient NO sensor system with low power consumption, which can deploy in a harsh environment.

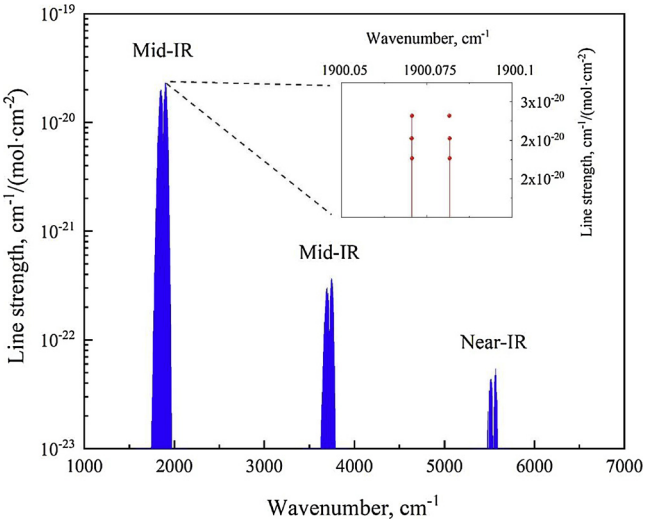

Fig. 1. Infrared absorption spectrum of NO based on HITRAN database. Inset: NO absorption doublet *R*(6.5) located at 1900.075 cm^{-1}.

2. NO sensor design

2.1. High temperature CW QCL

NO has its strong fundamental absorption lines in the mid-IR spectral range, which permits sensitive and selective trace NO detection. The targeted absorption line selection is depicted in Fig. 1. Based on the HITRAN database [10], the strong absorption doublet *R*(6.5) located at 1900.075 cm^{-1} offers access to NO transitions that are not affected by the water, carbon dioxide or carbon monoxide absorption in this spectral region. In fact, there are six NO absorption lines between 1900.065 cm^{-1} and 1900.085 cm^{-1} whose line strengths are higher than $2 \times 10^{-2°}$ cm/mol, as shown in the inset in Fig. 1. The six lines are so close that they are unresolved at atmospheric pressure [3].

To target the NO doublet *R*(6.5) at 1900.075 cm^{-1}, a high temperature CW DFB-QCL was designed and fabricated in the Institute of Semiconductors, China. The QCL utilizes a high efficiency active region structure based on an excited-states injection design [18]. A buried grating was fabricated in order to form a distributed feedback cavity. In order to improve the performance of QCL at high temperature, standard buried heterostructure processing was adopted [28]. A narrow ridge width of 7 μm was formed and a 5 μm-thick Au layer was electroplated on the upper electrode to improve thermal management. The 2 mm-long chip was mounted epi-layer down on an AlN heat sinks with AuSn solder. As a result, a high temperature stability can be ensured. The device was mounted into a commercial high heat load (HHL) style package to enhance the long-term performance of the QCL. Low-threshold continuous wave operation was achieved stably up to 70 °C.

The P-I-V (power-current-voltage) curves of the QCL were measured by means of a voltmeter (Agilent Technologies Model 3458 A) and an optical power meter (OPHIR Model NOVA II) as shown in Fig. 2(a). The QCL can be operated in a wide high temperature range from 40 °C to 70 °C and exhibits an excellent operating performance. A low threshold between 209 mA–285 mA was obtained depending on different operating temperatures. The maximum output power of the DFB-QCL was 44 mW at 40 °C with a threshold current density of 1.5 kA/cm^2 and a WPE of 1.4%, and then decreases to 6.5 mW when the temperature increases to 70 °C. The output wavelength of the DFB-QCL was characterized using a Fourier transform infrared (FTIR) spectrometer (Thermo Fisher Scientific Model Nicolet IS50), as shown in Fig. 2(b). Its wavelength can be tuned from 1898 cm^{-1} to 1902.5 cm^{-1}, which covers the wavelength range of the selected *R*(6.5) line plotted as a dotted black line. The current and temperature controlled wavelength

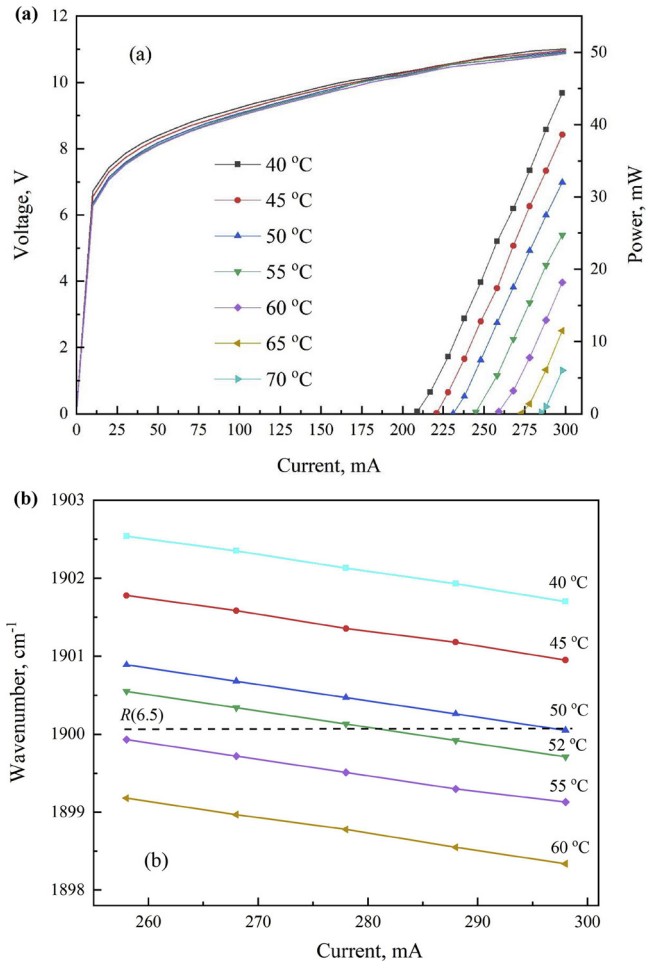

Fig. 2. (a) Power-current-voltage curves of a 5.26 μm CW DFB-QCL at different high temperatures; **(b)** The CW DFB-QCL emitted wavelengths as a function of injected current at different high temperatures.

tuning coefficients for this QCL were determined to be -0.02 cm^{-1}/mA and -0.18 cm^{-1}/°C, respectively. Based on Fig. 2(b), an operating temperature of 52 °C and a driving current of 283 mA were selected to reach the *R*(6.5) line. In this operating condition, the output power of the DFB-QCL is 24 mW.

2.2. Low-noise differential photoacoustic cell

A low-noise differential photoacoustic cell was designed to be couple with the CW DFB-QCL as shown in Fig. 3(a) and (b). A fully symmetrical geometry was developed in order to suppress the acoustic noise produced by gas flow in the gas-handling system, the absorbing species in the photoacoustic cell, such as windows and dust as well as the electromagnetic noise [23,29]. Two identical acoustic resonators were machined from stainless steel with 90 mm in length and 8 mm in diameter. The acoustic resonators were operated at the first longitudinal resonant mode near 1779 Hz with a *Q* factor of ˜27 in the standard air. Two microphones which have the same sensitivity at ˜1779 Hz were installed at the middle of two acoustic resonators, respectively, to detect the acoustic signal. The signals from the two microphones were amplified by a differential amplifier. The acoustic resonators were placed between four buffer volumes and four λ/4 filters. The four λ/4 filters had an inner radius of 8 mm, the same as the inner radius of the acoustic resonator, which allows the infrared beam to pass through easily. Each buffer volume had a length of 20 mm. The combination of buffer volume and λ/4 filter can efficiently suppress outside noise in the range of the first radial mode of the acoustic resonator. The

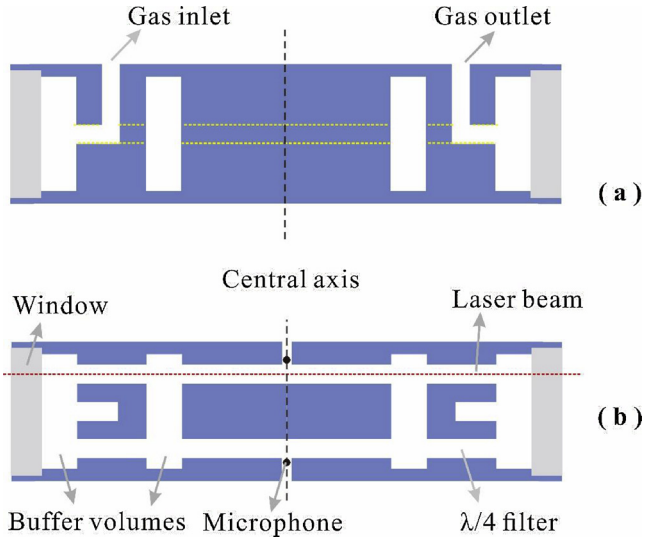

Fig. 3. Horizontal **(a)** and Vertical **(b)** cross section of the low-noise resonance system.

gas inlet was positioned between two neighboring λ/4 filters and between two neighboring buffer volumes. The gas outlet was symmetrically installed at the other side of the central axis of the photoacoustic cell, as shown in Fig. 3. Two calcium fluoride windows with a diameter of 60 mm were employed to seal the photoacoustic cell but allow access to the QCL beam. The gas flow passes through both acoustic resonators while the QCL beam irradiates only one of them. Thus the photoacoustic signal was generated in only one acoustic resonator, while the coherent noise components were produced in both acoustic resonators. Hence the photoacoustic signal can be retrieved and the coherent noise components can be eliminated via a differential operation of the signals from the two different microphones. The inner surface of the acoustic resonators, the buffer volumes as well as the filters were polished in order to further suppress the noise resulting from both reflected or scattered light in the acoustic resonators.

2.3. PAS sensor system

A PAS sensor system based on a high temperature CW DFB-QCL and a low-noise photoacoustic cell was developed for NO detection. The schematic of the sensor system is depicted in Fig. 4. The custom made CW DFB-QCL emitting at 5.26 μm was driven by a temperature controller (Thorlabs, Inc. Model TED200C) and a current supply (ILX Lightwave Model LDX-3232). The 2*f* wavelength modulation spectroscopy (2*f*-WMS) detection technique was adopted in order to improve the signal to noise (SNR) ratio of the sensor system [30,31]. The wavelength of the exciting laser was dithered by applying a sinusoidal modulation to the drive current at the half of the resonance frequency ($f_0/2$), while the signal amplified by the differential amplifier was detected at f_0 by means of a lock-in amplifier (LIA) (Stanford Research Systems Model SR830). A low-frequency (0.1 Hz) ramp was provided to scan the QCL current and obtain the NO photoacoustic spectrum. The sinusoidal modulation signal and the low-frequency scan signal were generated from the same function generator (Tektronix, Inc. Model AFG 3022). The QCL laser beam was first collimated by lenses which were part of the HHL package and then passed through one of the two acoustic resonators. The optical power of the QCL was monitored via a power meter (Ophir Optronics Solutions, Model 3A-ROHS), which was placed after the photoacoustic cell. The signal amplified by the differential amplifier was fed into the LIA mentioned above. The filter slope and the time constant of the LIA were set at 12 dB/oct and 300 ms, respectively, corresponding to a detection bandwidth of 0.833 Hz. An acquisition system consisting of a DAQ card and a laptop was used to

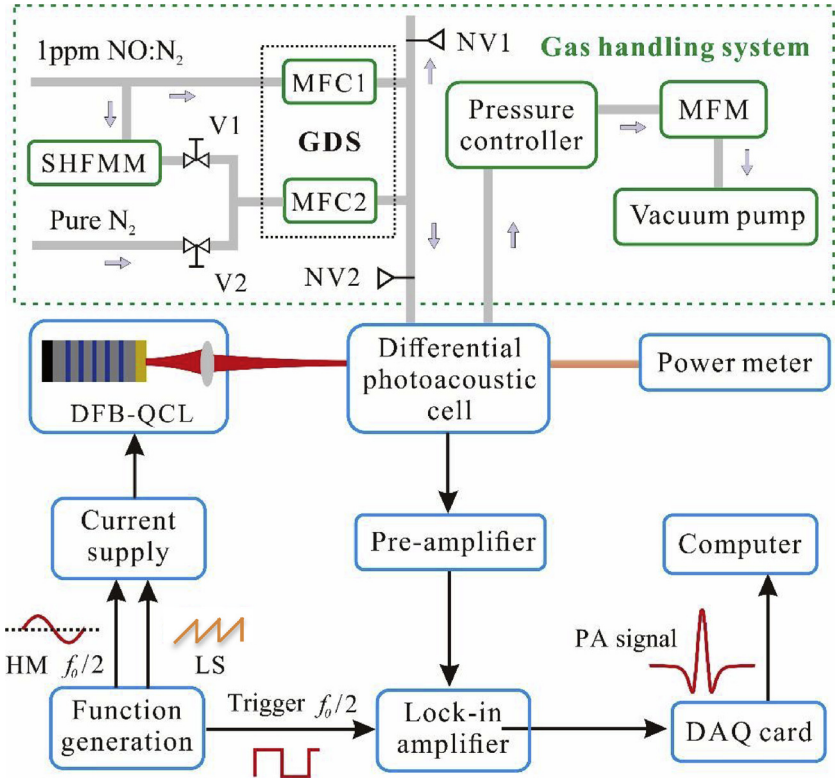

Fig. 4. Schematic of the NO photoacoustic sensor. GDS: gas dilution system; MFC: mass flow controller; V: valve; NV: needle valve; SHFMM: silicone hollow fiber membrane module; MFM: mass flow meter; HM: high-frequency modulation; LS: low-frequency scan; DAQ card: data acquisition card.

acquire the signal from the LIA. A LabView based routine was written in order to implement signal processing of the NO sensor system.

A gas handling system was used to optimize the sensor parameters. A gas dilution system (Environics, Inc. Model 4000) and a silicone hollow fiber membrane module (PermSelect Model PDMSXA-2500) were placed upstream to generate a NO: H_2O: zero air gas mixture by means of two valves (valve 1 and valve 2). Two needle valves were placed after the gas dilution system to adjust the gas flow rate. A mass flow meter (Alicat Scientific, Inc. Model M-2SLPM-D/5 M) and a vacuum pump (Oerlikon Leybold Vacuum Inc. Model D16C) were installed downstream to monitor the gas flow and provide the sensor system with negative pressure, respectively. The pressure of the gas in the photoacoustic cell was controlled and maintained by a pressure controller (MKS Instruments Inc. Model 649B13TS1M22 M).

3. Optimization and performance of the NO sensor system

3.1. Parameter optimization

The NO detection was based on a 2*f*-WMS approach by dithering and scanning the laser current, as described in Section 2.3. Hence the laser modulation depth must match the pressure-dependent absorption linewidth. The gas pressure and the laser wavelength modulation depth were optimized for achieving the highest 2*f* photoacoustic signal. The optimization was carried out with a 1 ppm NO: zero air mixture. The flow was set to 200 sccm. As the resonance frequency of the photoacoustic cell depends on the gas pressure, the modulation frequency was calibrated every time the gas pressure in the photoacoustic cell was changed. The peaks value of the 2*f* signals for the 1 ppm NO: zero air mixture for the different pressures are depicted in Fig. 5 as a function of the laser current modulation depth. The maximum photoacoustic signal was observed at 600 Torr with a current modulation depth of 14 mA. In fact, the maximum NO signal is only ~1% higher than the 760 Torr signal value with an 18-mA current modulation depth. It is more convenient to operate the PAS-based NO sensor at atmospheric pressure since in this case the sensor system can be simplified by removing the pressure controller [32]. Hence, further evaluation tests of the NO sensor were performed at atmospheric pressure with a 18 mA current modulation depth.

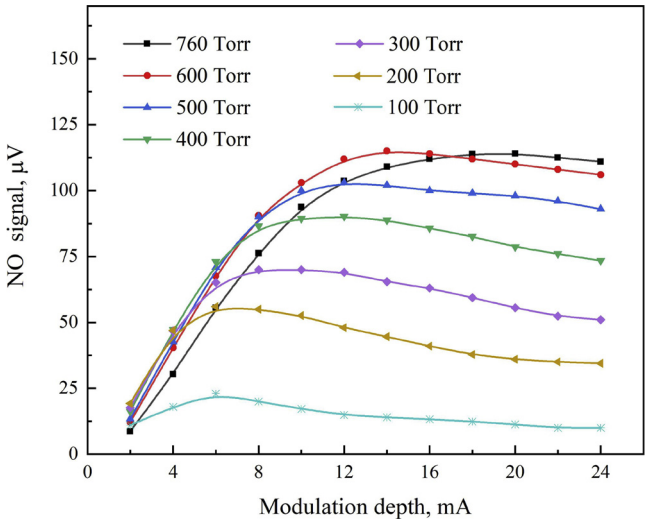

Fig. 5. A photoacoustic signal corresponding to the peak NO absorption near 1900.075 cm^{-1} for different gas pressures and laser current modulation depths. All measurements were performed with a 1 ppm NO: zero air mixture and with the CW DFB-QCL operating at 52 °C.

For a PAS-based sensor, the signal amplitude is strongly dependent on the vibration-to-translation (V—T) energy transfer time ($\tau_{v\text{-}t}$) of the target gas [33,34]. In case of slow V—T relaxation with respect to the exciting laser modulation frequency:

$$2\pi f \cdot \tau_{V\text{-}T} \gg 1 \quad (1)$$

the photoacoustic signal amplitude can be enhanced by adding relaxation promoters to the gas sample mixture. Water vapor is an efficient catalyst for the vibrational energy transfer reactions in the gas phase since it is an extremely fast relaxation molecule. The H_2O influence on the NO photoacoustic signal has been studied in detail by Spagnolo [3] and Dong [35] respectively. As mentioned in Ref 35, for quartz enhanced photoacoustic spectroscopy (QEPAS) based sensor, the NO signal amplitude can be increased by more than two orders of magnitude by adding water vapor. Furthermore, the existence of H_2O is unavoidable for many practical applications of NO detection, such as in automotive exhaust and environmental monitoring. Hence, an analysis of the effect of water vapor on the NO photoacoustic signal is essential for the sensor system reported in this work.

When wet zero air is used as the carrier gas, the V-T relaxation process of NO can be investigated via developing a V-T relaxation theoretical model in which only a one-stage collision is considered [36]. In this model, the obtained NO PAS signal $S_{PAS\text{-}NO}$ consists of three parts: the collision of NO and air gas molecules $S_{NO\text{-}Air}$, NO and H_2O molecules $S_{NO\text{-}H_2O}$, and NO and NO molecules $S_{NO\text{-}NO}$:

$$S_{PAS\text{-}NO} = S_{NO\text{-}Air} + S_{NO\text{-}H_2O} + S_{NO\text{-}NO} \quad (2)$$

Considering the low concentration of NO, the collisions of two NO molecules are neglected and Eq. (2) can be rewritten as the following equation:

$$S_{PAS\text{-}NO} = S_{NO\text{-}Air} + S_{NO\text{-}H_2O} = S_{NO\text{-}N_2}\left(1 + \frac{C_1}{\sqrt{1 + C_2/P_{H_2O}^2}}\right) \quad (3)$$

where C_1 and C_2 are constants and P^{H_2O} is the H_2O partial pressure. The C_1 value is determined by the two NO maximum signals obtained with the saturated water and in dry zero air, respectively. C_2 is determined by the resonance frequency of the photoacoustic cell and the relaxation time constant of NO. According to Eq. (3), the NO signal amplitude should rapidly increase with the increasing H_2O partial pressure at the beginning and then the growth trend of the $S_{PAS\text{-}NO}$ should become slower.

A certified mixture of 1 ppm NO in zero air was used for analyzing the influence of H_2O on the NO photoacoustic signal. The valve 1 shown in Fig. 4 was opened while valve 2 was closed completely. The mixture was divided into two gas lines. One gas line was humidified by means of a silicone hollow fiber membrane module. The wet and dry gas lines were connected to two mass flow controllers (MFCs), respectively, inside the gas dilution system. The maximum humidity is determined by the silicone hollow fiber membrane module, which is 2.3% at a flow rate of 200 sccm and room temperature. Different humidity levels can be obtained via adjusting the flows of the two MFCs. A chilled mirror hygrometer (Edgetech instruments Inc. Model 52,773) was used to measure the humidity of the NO: H_2O: zero air mixture gas. The experiments were carried out at 760 Torr in a H_2O concentration range from 0 to 2.3% as shown in Fig. 6. The NO signal amplitude increases gradually with an increasing H_2O concentration. When the H_2O concentration level is > 1.6%, the NO signal amplitude remains constant, which means that the signal is saturated. This is due to the fact that the relaxation time of NO in zero air with 1.6% water vapor is ~76 μs, according to the theoretical model of the NO V-T relaxation mentioned above. In this case, the Eq. (1) is not satisfied.

Fig. 7 depicts the NO signal comparison between 1 ppm NO in dry zero air and 1 ppm NO in zero air with a 2.3% addition of water vapor. A signal gain factor of 1.6 was obtained, which is lower than the improvement factor of 130 in a QEPAS sensor system [35]. This can be explained by the fact that our PAS sensor system has a ~20 times lower response frequency than that of the QEPAS system, thus enabling the PAS system to meet the saturated condition Eq. (1) with minimum assistance by the catalyst.

Therefore, a determination of the water concentration in the measured gas or a > 1.6% water vapor addition is necessary to eliminate the water vapor influence in applications, where the water vapor concentration varies significantly. A constant water concentration of 2.3% was added to the NO: zero air mixture in the evaluation tests of the NO sensor. For this purpose, the valve 1 in Fig. 4 was closed and the valve 2 was opened. The silicone hollow fiber membrane module was placed between needle valve 2 and the differential photoacoustic cell to humidify the mixture.

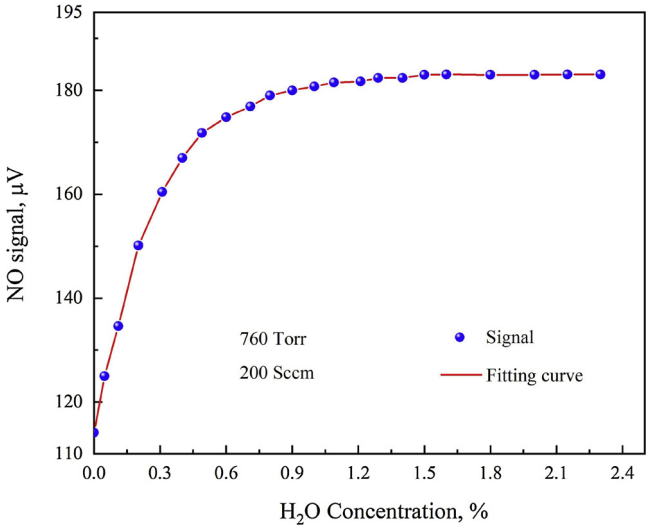

Fig. 6. PAS signal of NO as a function of added H_2O concentration. All measurements were performed at 760 Torr and with the CW DFB-QCL operating at 52 °C. The gas flow was set to 200 sccm.

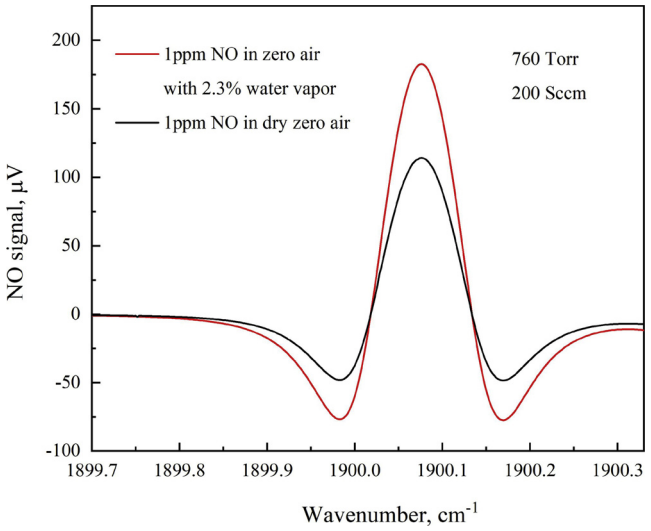

Fig. 7. Photoacoustic spectra of the NO absorption doublet at 1900.075 cm^{-1} in dry zero air (black line) and zero air with 2.3% water vapor (red line), respectively. (For interpretation of the references to colour in this figure legend, the reader is referred to the web version of this article).

3.2. Performance characteristics

Stepwise concentration measurements, a detection sensitivity calculation and an Allan–Werle deviation analysis were implemented to assess the performance of the NO sensor based on the high temperature CW DFB-QCL and the differential photoacoustic cell.

The linearity of the NO sensor was evaluated by measuring its response to different NO concentrations from 0 ppb to 1,000 ppb. The low-frequency ramp for wavelength scanning was disabled. The QCL

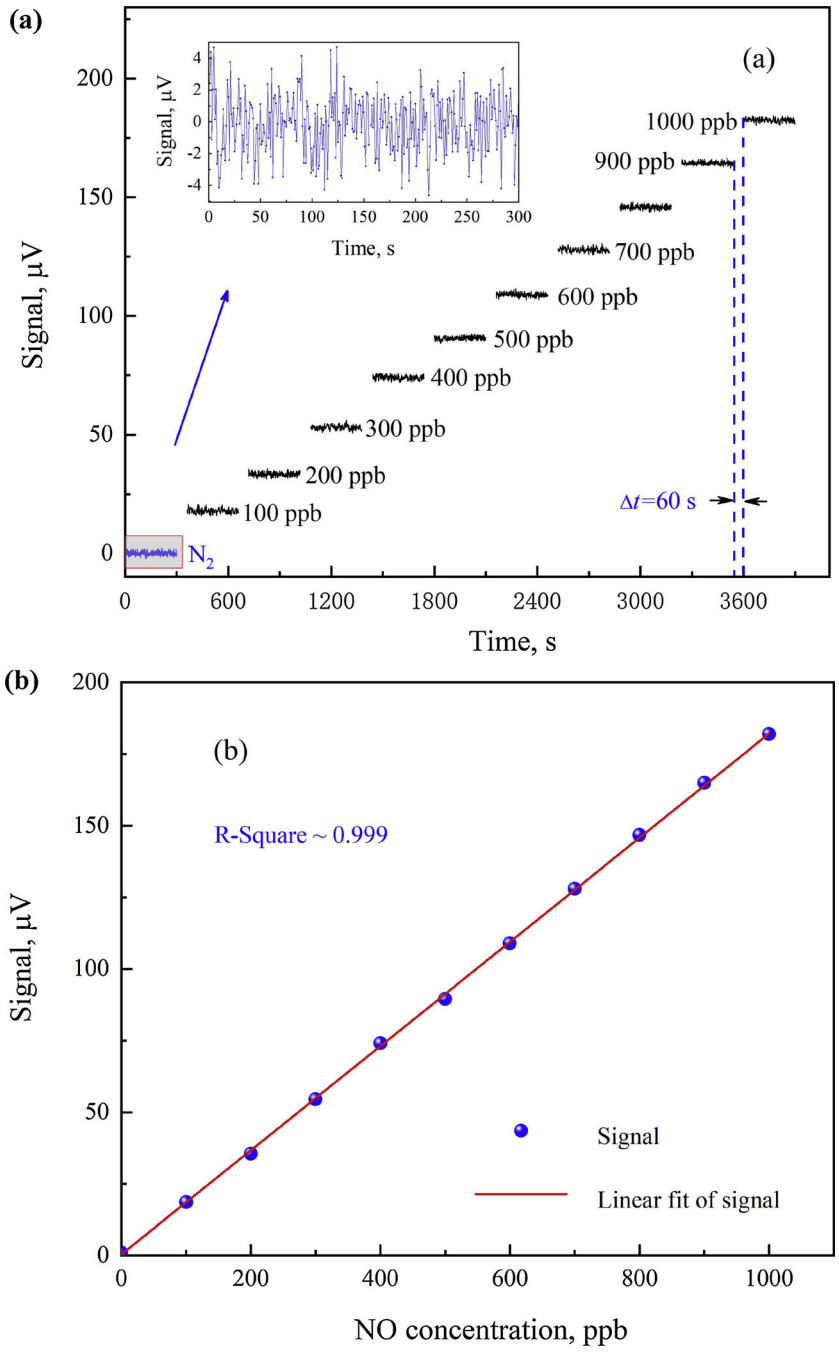

Fig. 8. (a) NO photoacoustic signal repetitively recorded as a function of time for NO concentration values ranging from 0 to 1 ppm. Inset: Enlarged image for the photoacoustic signal recorded as a function of time for pure zero air. **(b)** Same data averaged and plotted as a function of NO concentration.

wavelength was set to the peak of the *R*(6.5) absorption line. The integration time was set to 1 s. The results of repetitive measurements are plotted in Fig. 8(a). A 60-s interval between two adjacent concentration steps was set to replace the gas mixture in the photoacoustic cell with that with new concentration. The average values of the results for each step as a function of the NO concentrations were plotted in Fig. 8(b). A linear fitting procedure with a *R* square value of > 0.999, confirms the linearity of the sensor system response to NO concentration levels.

An enlarged image of the first concentration step was shown in the inset of Fig. 8(a), which depicts the background signal measured when the photoacoustic cell was filled with zero air. A noise level (1σ) of 1.45 μV occurred. Based on the noise level and the data depicted in Fig. 8(a), a 1σ minimum detection limit of 7 ppb was obtained for a 1-s integration time and with 24 mW QCL power. The corresponding normalized noise equivalent absorption (NNEA) coefficient for NO was determined to be 2.9×10^{-9} W•cm^{-1}/√Hz [37].

An Allan-Werle deviation analysis was performed when zero air with a 2.3% addition of water vapor was passed through the photoacoustic cell at atmospheric pressure for an investigation of the long term stability and precision of the NO sensor. Based on the Allan-Werle deviation plot shown in Fig. 9, the deviation follows a 1/√t dependence for time sequences over the entire duration of the measurement series (> 3,000 s), indicating a white noise behavior. Hence the detection limit can be significantly improved with a longer integration time. The optimal detection sensitivity can be reduced to the ppt level for a high temperature CW DFB-QCL based NO sensor when the integration time is longer than 100 s.

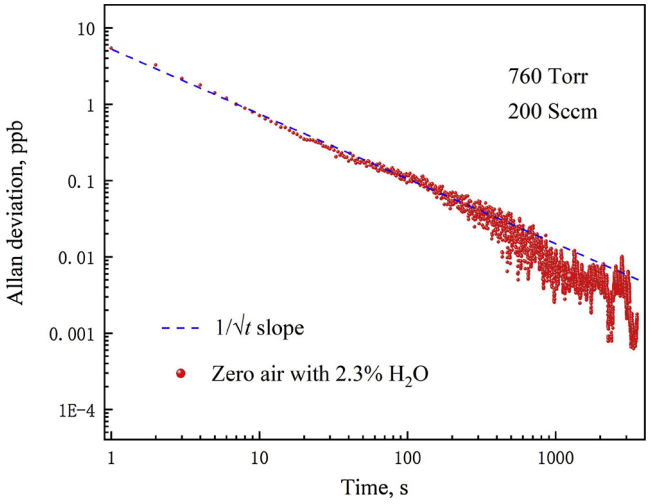

Fig. 9. Allan–Werle deviation as a function of the integration time. The measurements were performed at 760 Torr and with the CW DFB-QCL operating at 52 °C. Dashed line: 1/√t slope.

4. Outdoor monitoring of atmospheric NO concentration levels

The high temperature CW DFB-QCL based sensor system was employed for ambient NO monitoring from Dec. 29 to Dec.31. The sensor system was placed on the roof of the Shaw Amenities Building (37°47′59.1″N, 112°35′13.2″E) on the Shanxi University campus in Taiyuan, China. The NO sensor system was mounted inside a chamber, which was made from light-weight polymethyl methacrylate. The chamber was covered with thermal insulation material (Styrofoam) to reduce the heat transfer between the sensor system and environment. The temperature of the QCL was controlled by a TEC without the assistance of water chiller. The ambient air was sampled into the photoacoustic cell by a mini-diaphragm pump continuously.

A 3-μm micro-pore PTFE filter membrane was used at the front end of the sampling tube as the air filter to prevent contamination of the photoacoustic cell by dust or other particles existing in ambient air. The silicone hollow fiber membrane module was then directly used to add water vapor into the measured air, which results in ˜2.3% water content and thereby eliminates the influence of ambient water vapor on the V-T relaxation of NO molecule. The measured 2*f* spectrum was fitted to obtain the 2*f* signal amplitude using a Levenberg-Marquardt nonlinear least-squares fit procedure [38], which resulted in a data updating rate of 10 s with a detection sensitivity of ˜1 ppb.

The measured NO concentrations are shown in Fig. 10. The reported time period was selected because sustained haze weather conditions in Taiyuan (since Dec. 21) turned this region into an area of serious pollution. The heaviest haze and smog occurred on Dec. 29 and temporarily disappeared on Dec. 30 due to a strong wind lasting for an entire day. The haze and smog returned on Dec. 31 after the wind abated. In the absence of haze on Dec. 30, the NO concentration fluctuations can be explained by the photolysis process ($NO_2 + h\nu \rightarrow NO + O$) and the atmospheric chemistry reaction ($NO + O_3 \rightarrow NO_2 + O$, $O + NO + M \rightarrow NO_2 + M$, M: a molecule which can absorb the excess vibrational energy) as mentioned in Ref [39]. The NO concentration decreased rapidly from 0 a. m. to 8 a. m. (CST) on Dec. 30, which is mainly due to the fact that the high concentrations of NO gained in the sustained haze weather were diluted by strong wind. After 8 a. m., with an increase of the sunlight intensity, the photolysis process increased gradually the NO concentration. With decreasing sunlight intensity after 3 p. m., the atmospheric chemistry reaction gradually dominates, which resulted in a decrease of the NO concentration. The variation trend of the NO concentration on Dec. 31 is similar with that occurring on Dec. 29. The NO concentration increased for the first ˜8 h of the day, then dropped gradually to its lowest level trough at ˜1 p. m. and subsequently increased again until the end of the day. Multiple factors are responsible for a complicated behavior of the NO concentration fluctuations, including meteorology, coal burning by power and heating plants, photolysis, atmospheric chemistry reactions, traffic emissions as well as the haze [40]. Several sharp peaks related to motor vehicles activity were observed during measurements of the atmosphere air.

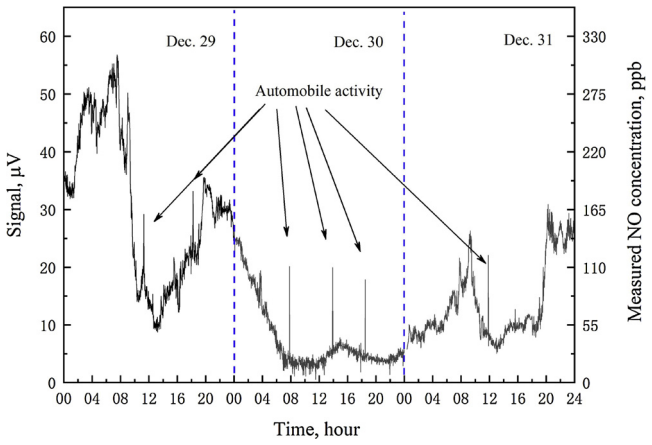

Fig. 10. Outdoor NO concentration monitoring on the Shanxi University campus, Taiyuan, China from Dec. 29 to Dec. 31.

5. Conclusions

A NO photoacoustic sensor system was developed for outdoor environmental monitoring. The sensor system employed a CW DFB-QCL operating at 52 °C. The operating capacity of the QCL at high temperature allows a totally thermoelectrically cooled mid-IR laser source with the advantages of low power consumption, a compact footprint and easy operation. A custom differential photoacoustic cell with a combination of λ/4 filters and buffer volumes was designed to match the high temperature QCL, resulting in a detection sensitivity of 7 ppb for a 1-s integration time and atmospheric pressure. The corresponding NNEA is 2. 9×10^{-9} W•cm^{-1}/√Hz, which is better than our previous report of a QCL based NO photoacoustic sensor in 2011 [35]. This verified the fact that the use of a totally thermoelectrically cooled CW QCL operating at high temperature in a NO photoacoustic sensor system does not result in a decrease of the sensor detection sensitivity. A higher detection sensitivity can be obtained by increasing the integration time as indicated in the Allan–Werle deviation analysis. Continuous monitoring of atmospheric NO for 72 h was performed to demonstrate the capability of the reported sensor system. A thermoelectrically cooled CW QCL operating at high temperature is important, especially for portable applications. Therefore our reported NO sensor results confirm a new approach for the design of hand-held or remotely deployed, battery-operated mid-IR QCL based sensor systems.

Acknowledgements

Lei Dong acknowledges support by National Key Research and Development Program of China (No. 2017YFA0304203); National Natural Science Foundation of China (Nos. 61622503, 61575113, 11434007); Changjiang Scholars and Innovative Research Team in University of Ministry of Education of China (No. IRTIRT_17R70); 111 project (Grant No. D18001), Outstanding Innovative Teams of Higher Learning Institutions of Shanxi; Shanxi “1331 Project”key subjects construction. Hongpeng Wu acknowledges support by Scientific Research Foundation (No. 227545028); National Natural Science Foundation of China (Nos. 61805132). Fengqi Liu and Jinchuan Zhang acknowledges support by National Natural Science Foundation of China

(Nos. 61435014, 61627822, 61574136 and 61774146). Frank K. Tittel acknowledges support by the US National Science Foundation (NSF) ERC MIRTHE award and the Robert Welch Foundation (Grant #R4925U).

References

[1] E. Culotta, D.E. Koshland, No news is good news, Science 258 (1992) 1862–1865.
[2] M. Jahjah, W. Ren, P. Stefański, R. Lewicki, J. Zhang, W. Jiang, J. Tarka, F.K. Tittel, A compact QCL based methane and nitrous oxide sensor for environmental and medical applications, Analyst 139 (2014) 2065–2069.
[3] V. Spagnolo, A.A. Kosterev, L. Dong, R. Lewicki, F.K. Tittel, NO trace gas sensor based on quartz-enhanced photoacoustic spectroscopy and external cavity quantum cascade laser, Appl. Phys. B 100 (2010) 125–130.
[4] A.R. Wellburn, Air Pollution and Climate Change, 2nd edn, Longman Scientific Technical, Harlow, UK, 1994, p. 186.
[5] Y. Yu, N.P. Sanchez, F. Yi, C. Zheng, W. Ye, H. Wu, R.J. Griffin, F.K. Tittel, Dual quantum cascade laser-based sensor for simultaneous NO and NO_2 detection using a wavelength modulation-division multiplexing technique, Appl. Phys. B 123 (2017) 164.
[6] M.W. Sigrist, Air Monitoring by Spectroscopic Techniques, Wiley & Sons, Inc., New York, 1994, pp. 163–220.
[7] A.A. Kosterev, A.L. Malinovsky, F.K. Tittel, C. Gmachl, F. Capasso, D.L. Sivco, J.N. Baillargeon, A.L. Hutchinson, A.Y. Cho, Cavity ring down spectroscopic detection of nitric oxide with a continuous-wave quantum-cascade laser, Appl. Opt. 40 (2001) 5522–5529.
[8] Y. Bakhirkin, A.A. Kosterev, C. Roller, R.F. Curl, F.K. Tittel, Mid-infrared quantum cascade laser based off-axis integrated cavity output spectroscopy for biogenic nitric oxide detection, Appl. Opt. 43 (2004) 2257–2266.
[9] L. Menzel, A.A. Kosterev, R.F. Curl, F.K. Tittel, C. Gmachl, F. Capasso, D.L. Sivco, J.N. Baillargeon, A.L. Hutchinson, A.Y. Cho, W. Urban, Spectroscopic detection of biological NO with a quantum cascade laser, Appl. Phys. B 71 (2001) 859–863.
[10] The HITRAN database, (2016) http://www.hitran.com.
[11] M.S. Cumis, S. Viciani, S. Borri, P. Patimisco, A. Sampaolo, G. Scamarcio, P.D. Natale, F.D. Amato, V. Spagnolo, A widely-tunable mid-infrared fiber-coupled quartz-enhanced photoacoustic sensor for environmental monitoring, Opt. Express 22 (2014) 28222–28231.
[12] M.W. Sigrist, Mid-infrared laser-spectroscopic sensing of chemical species, J. Adv. Res. 6 (2015) 529–533.
[13] M. Razeghi, Y. Bai, S. Slivken, S.R. Darvish, High-performance InP-based mid-infrared quantum cascade lasers at Northwestern University, Opt. Eng. 49 (2010) 111103.
[14] L. Dong, C. Li, N.P. Sanchez, A.K. Gluszek, R.J. Griffin, F.K. Tittel, Compact CH_4 sensor system based on a continuous-wave, low power consumption, room temperature interband cascade laser, Appl. Phys. Lett. 108 (2016) 011106.
[15] W. Ren, W. Jiang, F.K. Tittel, Single-QCL-based absorption sensor for simultaneous trace-gas detection of CH_4 and N_2O, Appl. Phys. B 117 (2014) 245–251.
[16] Y. Cao, N.P. Sanchez, W. Jiang, R.J. Griffin, F. Xie, L.C. Hughes, C. Zah, F.K. Tittel, Simultaneous atmospheric nitrous oxide, methane and water vapor detection with a single continuous wave quantum cascade laser, Opt. Express 23 (2015) 2121–2132.
[17] R. Lewicki, J.H. Doty lll, R.F. Curl, F.K. Tittel, G. Wysocki, Ultrasensitive detection of nitric oxide at 5.33 μm by using external cavity quantum cascade laser-based Faraday rotation spectroscopy, PNAS 106 (2009) 12587–12592.
[18] C. Liu, J. Zhang, F. Cheng, Y. Zhao, N. Zhuo, S. Zhai, L. Wang, J. Liu, S. Liu, F. Liu, Z. Wang, High efficiency quantum cascade lasers based on excited-states injection, IEEE Photonic. Technol. 30 (2018) 299–302.
[19] Y. Cao, W. Jin, L. Ho, Z. Liu, Evanescent-wave photoacoustic spectroscopy with optical micro/nano fibers, Opt. Lett. 37 (2012) 214–216.
[20] M.W. Sigrist, Trace gas monitoring by laser photoacoustic spectroscopy and related techniques (plenary), Rev. Sci. Instrum. 74 (2003) 486–490.
[21] V. Spagnolo, P. Patimisco, S. Borri, G. Scamarcio, B.E. Bernacki, J. Kriesel, Part-per-trillion level detection of SF_6 using a single-mode fiber-coupled quantum cascade laser and a quartz enhanced photoacoustic sensor, Opt. Lett. 37 (2012) 4461–4463.
[22] Z. Wang, Q. Wang, J.Y.L. Ching, J.C.Y. Wu, G. Zhang, W. Ren, A portable low-power QEPAS-based CO_2 isotope sensor using a fiber-coupled interband cascade laser, Sens. Actuators B Chem. 246 (2017) 710–715.
[23] A. Miklós, P. Hess, Application of acoustic resonators in photoacoustic trace gas analysis and metrology, Rev. Sci. Instrum. 72 (2001) 1937–1955.
[24] T. Starecki, A. Geras, Differential open photoacoustic Helmholtz cell, Int. J. Thermophys. 35 (2014) 2259–2268.
[25] M. Mordmüller, M. Köhring, W. Schade, U. Willer, An electrically and optically cooperated QEPAS device for highly integrated gas sensors, Appl. Phys. B 119 (2015) 111–118.
[26] Z. Li, Z. Wang, Y. Qi, W. Jin, W. Ren, Improved evanescent-wave quartz-enhanced photoacoustic CO sensor using an optical fiber taper, Sens. Actuators B Chem. 248 (2017) 1023–1028.
[27] T. Starecki, P.Z. Wieczorek, A high sensitivity preamplifier for quartz tuning forks in QEPAS (quartz enhanced photoacoustic spectroscopy) applications, Sensors 17 (2017) 2528.
[28] C. Hou, Y. Zhao, J. Zhang, S. Zhai, N. Zhuo, J. Liu, L. Wang, S. Liu, F. Liu, Z. Wang, Room temperature continuous wave operation of quantum cascade laser at λ ~ 9.4 μm, J. Semicond. 39 (2018) 034001.
[29] H. Zheng, M. Lou, L. Dong, H. Wu, W. Ye, X. Yin, C. Kim, M. Kim, W. Bewley, C. Merritt, C. Canedy, M. Warren, I. Vurgaftman, J. Meyer, F.K. Tittel, Compact photoacoustic module for methane detection incorporating interband cascade light emitting device, Opt. Express 25 (2017) 16761–16770.
[30] Y. Ma, Y. He, X. Yu, C. Chen, R. Sun, F.K. Tittel, HCI ppb-level detection based on QEPAS sensor using a low resonance frequency quartz tuning fork, Sens. Actuators B Chem. 233 (2016) 388–393.
[31] S. Schilt, L. Thevenaz, P. Robert, Wavelength modulation spectroscopy: combined frequency and intensity laser modulation, Appl. Opt. 42 (2003) 6728–6738.
[32] H. Wu, L. Dong, H. Zheng, X. Liu, X. Yin, W. Ma, L. Zhang, W. Yin, S. Jia, F.K. Tittel, Enhanced near-infrared QEPAS sensor for sub-ppm level H_2S detection by means of a fiber amplified 1582 nm DFB laser, Sens. Actuators B Chem. 221 (2015) 666–672.
[33] H. Wu, X. Yin, L. Dong, K. Pei, A. Sampaolo, P. Patimisco, H. Zheng, W. Ma, L. Zhang, W. Yin, L. Xiao, V. Spagnolo, S. Jia, F.K. Tittel, Simultaneous dual-gas QEPAS detection based on a fundamental and overtone combined vibration of quartz tuning fork, Appl. Phys. Lett. 110 (2017) 121104.
[34] X. Yin, L. Dong, H. Zheng, X. Liu, H. Wu, Y. Yang, W. Ma, L. Zhang, W. Yin, L. Xiao, S. Jia, Impact of humidity on quartz-enhanced photoacoustic spectroscopy based CO detection using a Near-IR telecommunication diode laser, Sensors 16 (2016) 162.
[35] L. Dong, V. Spagnolo, R. Lewicki, F.K. Tittel, Ppb-level detection of nitric oxide using an external cavity quantum cascade laser based QEPAS sensor, Opt. Express 19 (2011) 24037–24045.
[36] A.A. Kosterev, Y.A. Bakhirkin, F.K. Tittel, S. Mcwhorter, B. Ashcraft, QEPAS methane sensor performance for humidified gases, Appl. Phys. B 92 (2008) 103–109.
[37] H. Wu, L. Dong, H. Zheng, Y. Yu, W. Ma, L. Zhang, W. Yin, L. Xiao, S. Jia, F.K. Tittel, Calibration-free fast quartz-enhanced photoacoustic spectroscopy based on beat frequency effect for continuous trace gas monitoring, Nat. Commun. 8 (2017) 15331.
[38] J.J. Moré, The levenberg-marquardt algorithm: implementation and theory, Numerical Analysis, Springer, Berlin, Heidelberg, 1978, pp. 105–116.
[39] K. Liu, R. Lewicki, F.K. Tittel, Development of a mid-infrared nitrogen dioxide sensor based on Faraday rotation spectroscopy, Sens. Actuators B Chem. 237 (2016) 887–893.
[40] G. Wang, R. Zhang, M.E. Gomez, Lo Yang, M.L. Zamora, M. Hu, Y. Lin, J. Peng, S. Guo, J. Meng, J. Li, C. Cheng, T. Hu, Y. Ren, Y. Wang, J. Gao, J. Cao, Z. An, W. Zhou, G. Li, J. Wang, P. Tian, W. Marrero-Ortiz, J. Secrest, Z. Du, J. Zheng, D. Shang, L. Zeng, M. Shao, W. Wang, Y. Huang, Y. Wang, Y. Zhu, Y. Li, J. Hu, B. Pan, L. Cai, Y. Cheng, Y. Ji, F. Zhang, D. Rosenfeld, P.S. Liss, R.A. Duce, C.E. Kolb, M.J. Molina, Persistent sulfate formation from London Fog to Chinese haze, Proc. Natl. Acad. Sci. India A 113 (2016) 13630–13635.